The Fourth IEEE RAS/EMBS International Conference
on Biomedical Robotics and Biomechatronics
Roma, Italy. June 24-27, 2012

An optical 3D force sensor for biomedical devices

Lucas Samuel Lincoln, Morgan Quigley, Brandon Rohrer, Curt Salisbury, and Jason Wheeler

***Abstract*— In this paper we describe the development of an optical sensor that is low profile, inexpensive, physically robust, and suitable for contact with soft tissue. It is constructed using commercially available integrated circuits, a printed circuit board, and layers of silicone elastomer. The sensor exhibits modest drift and hysteresis, as well as some temperature sensitivity, for which we compensate. We demonstrate how the raw sensor signals can be used to infer both normal and shear forces. The sensor proves to be particularly sensitive to shear forces, reporting them accurately and with minimal coupling between them.**

I. INTRODUCTION

Low profile tactile sensors have been proposed for many applications including robot hands and skins [1], [2], [3] and biomechanical sensing at human/machine interfaces (e.g. in prosthetic sockets [4]). Many different types of tactile sensors have been proposed, including force sensitive resistors, which are available commercially, capacitive [4], optical [3], [2] and MEMS sensors. A recent review of tactile sensing can be found in Cutkosky, et al. [5].

The vast majority of the sensors in the research and patent literature sense normal loads (loads perpendicular to the sensing surface) but not shear loads (loads parallel to the sensing surface). For many applications, it would be beneficial to sense both. For instance in robotic hands, shear information could be used to improve object manipulation and tactile exploration. This information has also been shown to be important in monitoring prosthetic socket interface loads [6]. Multi-axis sensing has been primarily accomplished using traditional strain gauge-based load cells, which are typically large and expensive.

Several three-axis tactile sensors have been proposed. Capacitive sensors have been designed to infer shear information of overlapping conductors through a dielectric [4]. MEMS systems have been constructed with small cantilevers with piezo-resistive traces embedded in an elastomer [7], [8], [9]. These sensors have good sensing performance but have relatively small load capacity and are frail. Optical shear sensors have also been proposed. Missinnee et al. use a Vertical-Cavity Surface Emitting Laser which is mechanically separated from a photodiode by a silicone layer so that the two are displaced relative to one another by shear loads [10]. This sensor cannot sense normal pressure or easily differentiate between the two shear axes.

LS Lincoln is a student in the Bioinstrumentation Lab at the University of Utah, Salt Lake City, UT lucas.lincoln@utah.edu

M Quigley is a Ph.D. student in the AI Lab at Stanford University, Stanford, CA mquigley@cs.stanford.edu

B Rohrer, C Salibury, and J Wheeler are with Sandia National Laboratories, Intelligent Systems & Controls, Albuquerque, NM {rohrer, cmsalis, jwwheel}@sandia.gov

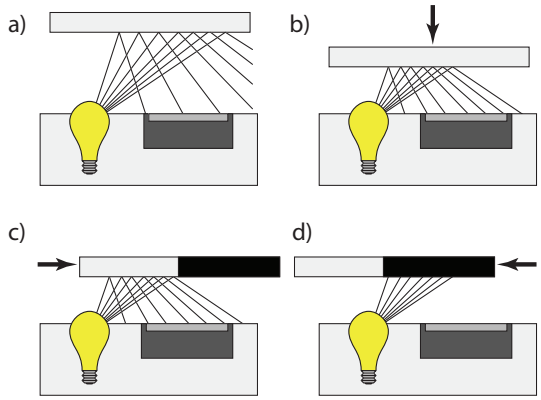

Fig. 1. The optical sensor's operating principle. a)-b) Normal loads move the reflective surface closer to the emitter, increasing the intensity of the light at the detector. c)-d) Shear loads move the absorptive portion of the polymer relative to the emitter, changing the intensity of the light at the detector.

In the present work, we present a three-axis optical sensor design which makes both normal and shear measurements. The sensor consists of small, inexpensive, surface-mount integrated circuits with multiple layers of silicone elastomer and is well suited for applications where a compliant material covers a rigid body (e.g. robot skins or prosthetic sockets).

II. SENSOR DESIGN

A. Principle of Operation

The sensor uses reflected light intensity to detect the proximity of a reflective material. As a normal load is applied to the reflective material, the interstitial transparent material compresses and the reflective material moves closer to the light source (emitter) and light sensor (detector). This causes the detector to detect increased reflected light from the emitter. (See Fig. 1a and 1b) Shear loads are sensed by adding absorptive regions to the reflective layer. An applied shear load changes the ratio of absorptive to reflective material between the emitter and the detector. The changes the amount of light reflected back to the detector. (See Fig. 1c and 1d)

Because each sensor configuration only provides information about a single degree of freedom, a *taxel* (from "tactile pixel") that provides three axes of information requires at least three sensors. Deducing the direction and magnitude of applied loads is most straightforward if the directional sensitivities of the three axes are independent.

B. Hardware and Implementation

The light emission and sensing were achieved using a photomicrosensor (EE-SY199, Omron Corporation, Kyoto,

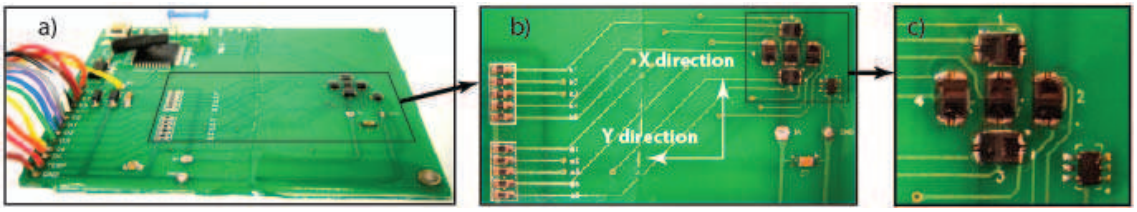

Fig. 2. Photograph of a five-sensor taxel (tactile sensing pixel). a) The entire printed circuit board, containing the sensors and the signal conditioning and preprocessing electronics. b) The sensors and their resistors. c) The photomicrosensor array, after coating with epoxy, but before coating with silicone. The center sensor is number 5. The chip to the lower right is a temperature sensor.

Japan) which contains both an infrared LED and phototransistor in the same package. This component was selected for its small size (approximately 3.2mm x 1.7mm x 1.1mm), wide-angle detection field, and the fact that its peak sensitivity occurs at approximately 1mm. We constructed a three-axis sensor consisting of five of these sensors: one which detected normal loads, two which detected shear in one direction, and two which detected shear in an orthogonal direction. (See Fig. 2) Initial characterization focused on the output from three of these sensors (2, 3, and 5), the simplest functional embodiment of the system. Initial data suggested that the redundant data provided by the additional two sensors did not greatly improve accuracy. These sensors were cast in clear epoxy (ES1902 Hysol, Locktite, Henkel, Düsseldorf, Germany) up to the height of their top surface. A 1mm thick layer of transparent silicon (Dragon Skin Fast, Smooth-On, Inc., Easton, Pennsylvania) was used for the transparent resilient material. A thickness of 1mm of the same material was used for the opaque material, with a white die (White Silc Pig, Smooth-On, Inc., Easton, Pennsylvania) added to create the reflective surfaces and a black die (Black Silc Pig, Smooth-On, Inc., Easton, Pennsylvania) added to create the absorptive surfaces. A 6mm square was chosen for the geometry of the absorptive-reflective boundary. The reflective square was centered over the sensor for detecting normal loads. Two orthogonal boundaries of the square were placed directly over the two shear sensors (see Fig. 3). The opaque silicone was cast on top of the transparent silicone. Because the materials were similar silicone formulations, the interface bond was excellent. The silicone assembly was then bonded to the clear epoxy with a clear instant adhesive (Loctite 403, Henkel, Düsseldorf, Germany). Based on each sensor's field of view, it is estimated that taxels can be as close as 9 mm from center to center.

The datasheet for the sensor suggests a 4mA drive current for the LED. Given a supply voltage of 5V and a voltage drop across the LED of 1.2V, we used a 1kΩ current-limiting resistor in series with the LED to set the LED drive current to 3.8mA. We found through experiment that a load resistance of 100kΩ for the phototransistor with a 5V supply voltage gave us maximum sensitivity without saturating.

The sensors within a given taxel were close enough to one another that each phototransistor detected the cumulative reflected light from all of the LEDs. This secondary illumination saturated the phototransistors. To address this,

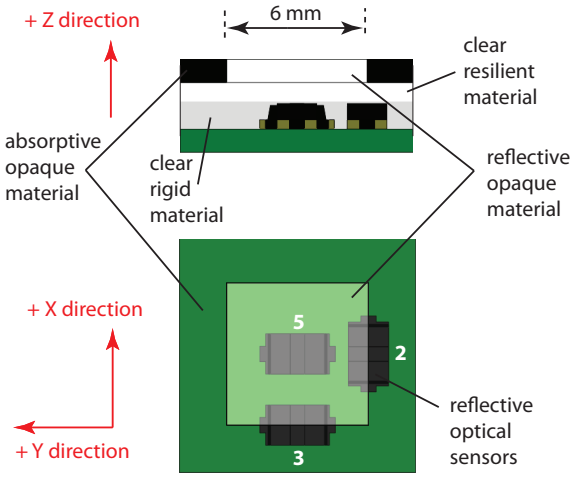

Fig. 3. Physical configuration of a single three-sensor taxel (sensors 1 and 4 from Figure 2 omitted). Changes in the reflected light intensity at the sensors allow measurement of normal and shear loads in three axes.

we only drove one emitter at a time. The response time of the phototransistor was dependent upon the phototransistor load resistance. Our 100kΩ resistor caused an exponential transient response with a 100μs time constant. In order to capture an accurate measurement from the phototransistor, we needed to wait until the phototransistor signal settled. Consequently, we set the LED pulses to be 1ms long. The phototransistor signal was sampled at 400μs, 500μs, 600μs and 700μs, and these four samples were averaged to generate a single phototransistor measurement (see Fig. 4). A single taxel measurement required measuring all three of the sensors and took a total of 3ms.

III. SENSOR CHARACTERIZATION

A. Method and Apparatus

A sensor designer and integrator is concerned about a variety of sensor characteristics when selecting a sensor for a particular application. We characterized several of these: the load sensitivity, hysteresis, drift, temperature sensitivity, and dynamic response of the prototype tactile sensor. All data were captured at 10kHz through a 16-bit National Instruments DAQ board (NI-PCI6229, National Instruments, Austin, TX). The data included the three photodetector analog signals and the three binary emitter states.

1) Load Sensitivity: We characterized the sensitivity of each of the three sensors in the taxel to normal and shear

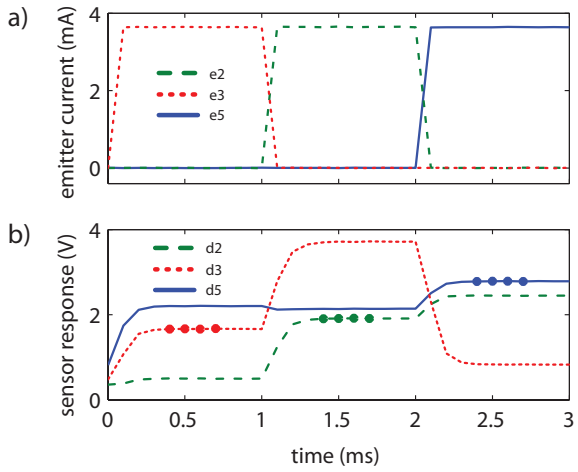

Fig. 4. Emitter-detector intensities. a) The LEDs were driven sequentially (emitter 3, emitter 2, then emitter 5). b) The photodetectors sensed the reflected intensity due to each. Note that in some instances another detector responded more strongly to an emitter than its own. (See for instance detector 3's response to emitter 2, the center plateau in the red trace.) Dots indicate the samples used to calculate a sensor value.

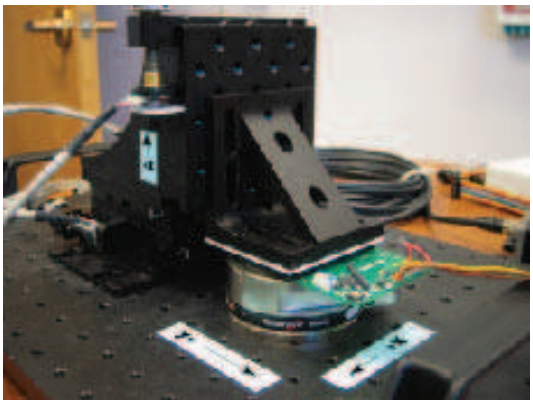

Fig. 5. The testing apparatus, including a three-axis linear stage, six-axis force transducer, and printed circuit board containing the three-axis tactile sensor.

loads. To apply and measure shear and normal loads, we built and designed a test fixture (see Fig. 5) which consisted of a three-axis linear stage (LT3, Thorlabs, Newark, NJ) attached to an optical breadboard and retrofitted with three optical encoders (S4-360-125-B-D, US Digital, Vancouver, WA) to record linear translation of the three stages ($<1\mu$m resolution). The optical encoder signals were sampled at 10kHz using a USB data-acquisition device (PhidgetEncoder, Phidgets, Calgary, Alberta, Canada). A six-axis load cell (Gamma US-30-100, ATI Industrial Automation, Apex, NC) was also rigidly attached to the breadboard, and the force and torque data were recorded through the same 16-bit NI DAQ board. The three-axis tactile sensor was mounted on top of the load cell. An effector plate attached to the stage applied loads to the top of the optical sensor through manual control of the linear stages.

Using this apparatus, we cycled stage displacements of approximately 1mm in a single direction (e.g. along the normal axis or one of the shear axes) at a time. Cycles were generated for all three directions and the sensor response was compared to the measured forces.

2) Cyclic Drift: To characterize the drift of the taxel output over time when driven by a cyclic load, we placed it in a single-axis load frame (MTS Systems Corp., Cary, NC) and loaded it in the normal direction. The load was cycled from 32 to 180kPa in a 0.5Hz triangle wave for approximately 2 hours. The MTS machine load cell data was recorded on the NI DAQ card.

3) Static Drift and Temperature Sensitivity: To characterize the static drift of the taxel, a 67N load with a contact area of 645mm^2 was placed on it, resulting in a sustained normal load. The sensor data were recorded for a period of 16 hours. Ambient thermal data were also recorded on the NI DAQ card.

4) Dynamic Response: To characterize the dynamic response of the taxel, it was positioned in a vise such that closing the jaws applied a normal load. The vice was then quickly closed on the taxel, resulting in a step-like response. Only sensor 5 was measured, with only its emitter on, for the duration of the experiment. In this fashion, we ensured that the sample rate was not limited by the serial sampling scheme for the three sensors.

5) Sensor modeling: With basic sensor characterization complete, data from all five sensors on the board were gathered for testing and validation. A five sensor arrangement resulted in a similarly sized taxel but provided redundant sensors for sensing shear, possibly increasing accuracy. Although the emitters were active only in pulses, the detectors were on continuously. The light from a single emitter could reach multiple detectors, providing additional information. With five sensors, each emitter pulse provided five values, and an entire pulse train (5ms at 1ms/pulse with five sensors) provided 25 signals. All 25 emitter-detector signals were captured while the sensor was subjected to complex three-dimensional loads. The system was trained using a linear-least-squares regression to determine coefficients (α) of the linear model:

$$\begin{aligned} p_x &= \alpha_{x1}D_1E_1 + \alpha_{x2}D_1E_2 + \alpha_{x3}D_1E_3 + ... \\ &\quad \alpha_{x23}D_5E_3 + \alpha_{x24}D_5E_4 + \alpha_{x25}D_5E_5 + \alpha_{x26} \\ p_y &= \alpha_{y1}D_1E_1 + \alpha_{y2}D_1E_2 + \alpha_{y3}D_1E_3 + ... \\ &\quad \alpha_{y23}D_5E_3 + \alpha_{y24}D_5E_4 + \alpha_{y25}D_5E_5 + \alpha_{y26} \\ p_z &= \alpha_{z1}D_1E_1 + \alpha_{z2}D_1E_2 + \alpha_{z3}D_1E_3 + ... \\ &\quad \alpha_{z23}D_5E_3 + \alpha_{z24}D_5E_4 + \alpha_{z25}D_5E_5 + \alpha_{z26} \end{aligned} \quad (1)$$

In the model notation, D_iE_j is the signal from detector i while illuminated by emitter j. Other models were tested as well: non-linear polynomial models up to the 3rd order and models incorporating the slope of the incoming signals. Performance was most consistent across trials with the linear least squares regression of Equation 1. For comparison, two reduced-order models were assessed as well. In a 5 signal model (Equation 2), detectors only reported on measurements made while their own emitter was active. These signals

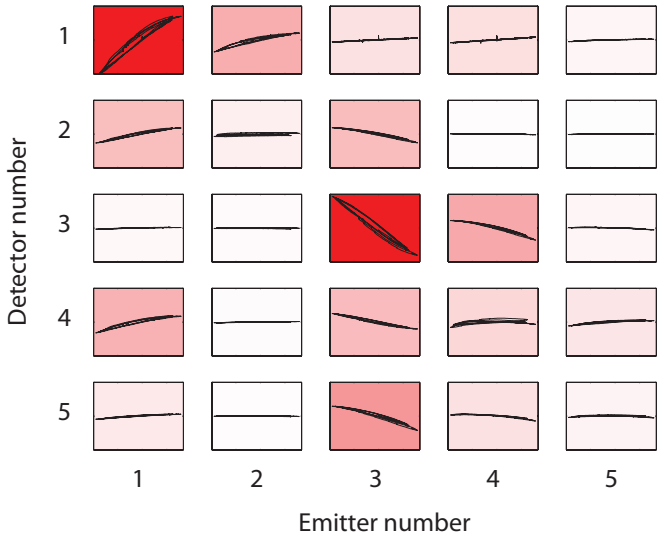

Fig. 6. Signal response to changing x load. Rows are detectors; Columns are emitters. x axis is pressure; y axis is signal voltage. Background color intensity represents sensitivity, also visible in the overall slope of each line.

typically appeared to be the largest in magnitude and the most sensitive to changes in load.

$$\begin{aligned} p_x &= \alpha_{x1}D_1E_1 + \alpha_{x2}D_2E_2 + \alpha_{x3}D_3E_3 + \\ &\quad \alpha_{x4}D_4E_4 + \alpha_{x5}D_5E_5 + \alpha_{x6} \\ p_y &= \alpha_{y1}D_1E_1 + \alpha_{y2}D_2E_2 + \alpha_{y3}D_3E_3 + \\ &\quad \alpha_{y4}D_4E_4 + \alpha_{y5}D_5E_5 + \alpha_{y6} \\ p_z &= \alpha_{z1}D_1E_1 + \alpha_{z2}D_2E_2 + \alpha_{z3}D_3E_3 + \\ &\quad \alpha_{z4}D_4E_4 + \alpha_{z5}D_5E_5 + \alpha_{z6} \end{aligned} \tag{2}$$

In a further reduced model, only three signals were used. (Equation 3) As can be seen in Figure 2, there were two sensors positioned to measure shear in the x-direction and two more for the y-direction. In the three sensor model, two of the redundant sensors were ignored.

$$\begin{aligned} p_x &= \alpha_{x1}D_2E_2 + \alpha_{x2}D_3E_3 + \alpha_{x3}D_5E_5 + \alpha_{x4} \\ p_x &= \alpha_{y1}D_2E_2 + \alpha_{y2}D_3E_3 + \alpha_{y3}D_5E_5 + \alpha_{y4} \\ p_x &= \alpha_{z1}D_2E_2 + \alpha_{z2}D_3E_3 + \alpha_{z3}D_5E_5 + \alpha_{z4} \end{aligned} \tag{3}$$

B. Results

1) Load Sensitivity: Figure 7 shows the response of the three sensors to loads in x (shear), y (shear), and z (normal). Sensor 3 had a sensitivity of approximately -15.7mV/kPa to shear loads in x while sensors 5 and 2 had sensitivities of approximately 0mV/kPa and 0.7mV/kPa, respectively. Sensor 2 had a sensitivity of approximately -19.4mV/kPa to shear loads in y while sensors 5 and 3 both had sensitivities of approximately 0mV/kPa. Sensor 5 had a sensitivity of approximately -0.58mV/kPa to normal loads in z while sensors 2 and 3 had sensitivities of approximately -0.44mV/kPa and -0.96mV/kPa, respectively, although both contained significant nonlinearities in their responses to moderate normal loads. The hysteresis of sensors 2, 3, and 5 was approximately 10%, 9%, and 7%, respectively.

2) Cyclic Drift: Figure 8a shows the response of sensor 5 to 10 loading and unloading cycles at the beginning of the cyclic drift test and 10 loading and unloading cycles at the end of the test. The sensor response drifted approximately 50mV over the 2 hour test. The sensitivity at the beginning was -0.28mV/kPa and the sensitivity at the end was -0.26mV/kPa. The taxel used for this test was of slightly different construction than that used for the sensitivity measurements, and had a lower sensitivity to normal loads.

3) Static Drift and Thermal Sensitivity: Figure 8b shows the response of sensor 5 to a static load over approximately 16 hours. The sensor response drifted approximately 32mV over the 16 hour test. Figure 8c shows the same data as a function of ambient temperature. The sensor had a thermal sensitivity of approximately 11mV/°C. This is consistent with the value found on the datasheet for the sensor. Figure 8b also shows the static drift when temperature effects were removed. In this case, the static drift was approximately 4mV.

4) Dynamic Response: Figure 8d shows the response of sensor 5 to a step-like load in time and the z axis load as measured by the ATI force sensor. The load reflects the contact pressure on the top surface of the silicone, while the sensor voltage reflects the translation of an internal, reflective boundary. Two notable features of data can be explained by viscoelastic effects: 1) sensor 5 lagged the ATI signal on the upward slope of the curve and 2) the ATI signal relaxed by approximately 10kPa on the plateau.

5) Modeling results: Figure 6 demonstrates the sensitivities of each of these terms to a varying x load at a fixed normal pressure. Plots in a row in this figure are from a common detector; and plots in a column are from a common emitter. Plots on the diagonal represent the self emitter/detector signal (those signals which were characterized in the previous section of this paper). Off-diagonal terms are detector responses to other emitters. The figure demonstrates that some of the non-self emitter/detector combinations provide information to shear forces, and, though less sensitive than the self-illuminated terms, may contribute to the more accurate measurement of force.

All 78 coefficients in the 25-signal model (Eq. 1) were calculated using data collected during one trial, and the model's accuracy was evaluated by applying the coefficients obtained to the data from a second trial. The optical sensor signals recorded during the validation trial were used as inputs to the model, and the pressure predicted by the model was compared against that measured with the load cell. A characteristic comparison is shown in figure 9, showing optical sensor results along with load cell results. Shear determination was accurate to an root-mean-square (rms) error of 2.4kPa in x and 3.2kPa in y for the representative trial displayed in figure 9. The rms error for the normal pressure was 11.4kPa.

The coefficients for the five signal (Eq. 2) and three signal models (Eq. 3) were calculated as well. The data collected for evaluating the reduced-order models was different than the data collected for evaluating the 25 signal model in several ways. For the reduced-order models, the forces

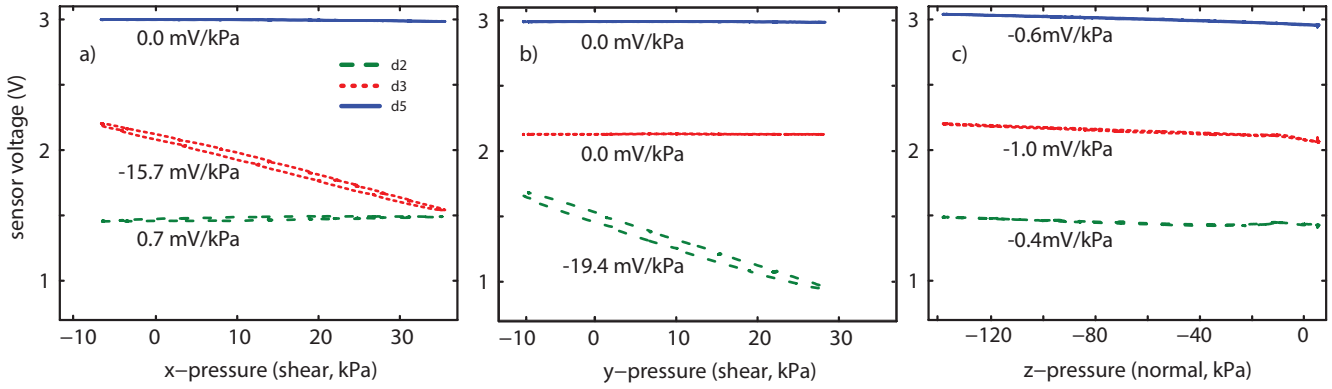

Fig. 7. Sensor responses to loading in the directions indicated, with approximate sensitivities.

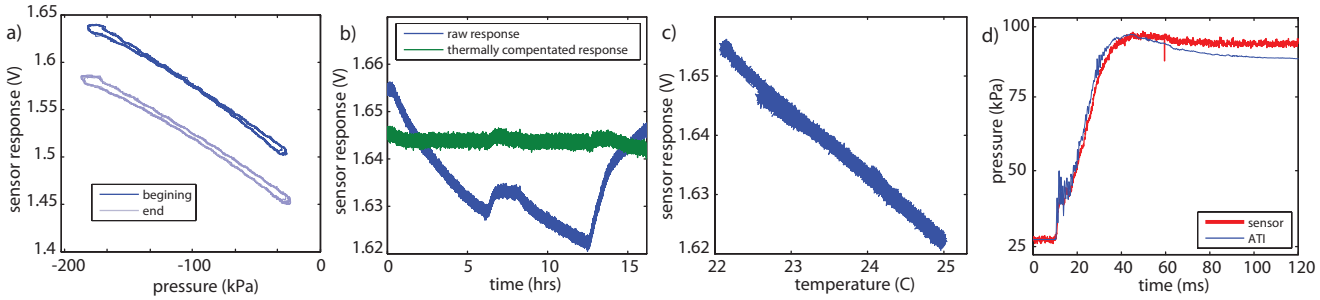

Fig. 8. a) Sensor 5 response to cycling in the z (normal) axis. 10 cycles at the beginning of the test (dark blue) differ from 10 cycles after approximately 2 hours (light blue). b) Sensor 5 response in time subject to a static load in the z-axis. c) Sensor 5 response to changes in ambient temperature. d) Sensor 5 response in time to a step-like load in the z-axis and the z-axis load as measured by the ATI force sensor.

model	25 signal	5 signal	3 signal
x (shear) error	2.4 kPa	4.0 kPa	4.4 kPa
y (shear) error	3.4 kPa	5.3 kPa	5.6 kPa
z (normal) error	11.4 kPa	12.6 kPa	12.6 kPa

TABLE I

MODELING ERRORS IN EACH OF THREE AXES.

were applied by hand, rather than by turning the knobs on a three-axis stage. This resulted in data that was more complex (it changed simultaneously in multiple axes) and of lower magnitude (the stages had greater force-production capabilities than the investigators' hands). While this made direct comparison between the data challenging, it did result in data with characteristics similar to those expected in robotics and prosthetics applications. Additional differences were introduced in the analysis of the data. For the reduced-order models, 10 data sets were collected, and the models were evaluated using leave-one-out-cross-validation. They were trained on 9 of the data sets, and tested on the tenth, and this process was repeated for each of the ten data sets. The results were then averaged together.

As a result of these differences, comparisons between the 25 signal model and the reduced-order models must be made with caution. However, comparison is still instructive. The error in all three models is summarized in Table I.

The reduced-order models showed a somewhat lower performance (higher rms error) than the full 25 signal model. This is not surprising, since the 25 signal model makes use of more information, although for reasons mentioned earlier care should be taken in interpreting this difference. Particularly interesting is the comparison between the five signal and three signal models. The performance difference is relatively small, even indistinguishable in the case of normal loads.

C. Discussion

The taxel's sensitivity in measuring shear suggests that it may be a viable sensor for use in robotic and prosthetic tactile sensing applications. Its normal sensitivity was more than an order of magnitude lower. Its potential usefulness as a sensor for normal loads has yet to be established, however our experience with the device gives encouragement that its normal sensitivity can be improved and its error in predicting normal forces decreased.

The taxel drifted about 35kPa over the course of 2 hours of cyclic loading. Though we did not record temperature during this experiment, the information we gathered from the static drift experiment leads us to believe that the cyclic drift observed was largely due to temperature. During the static drift experiment, we measured the ambient temperature and the data show that the drift observed can be attributed almost entirely to thermal fluctuation. We suspect that by incorporating the taxel's thermal sensor into the postprocessing of its sensor measurements, we can eliminate the cyclic and static drift. As shown in the characterization of the dynamic

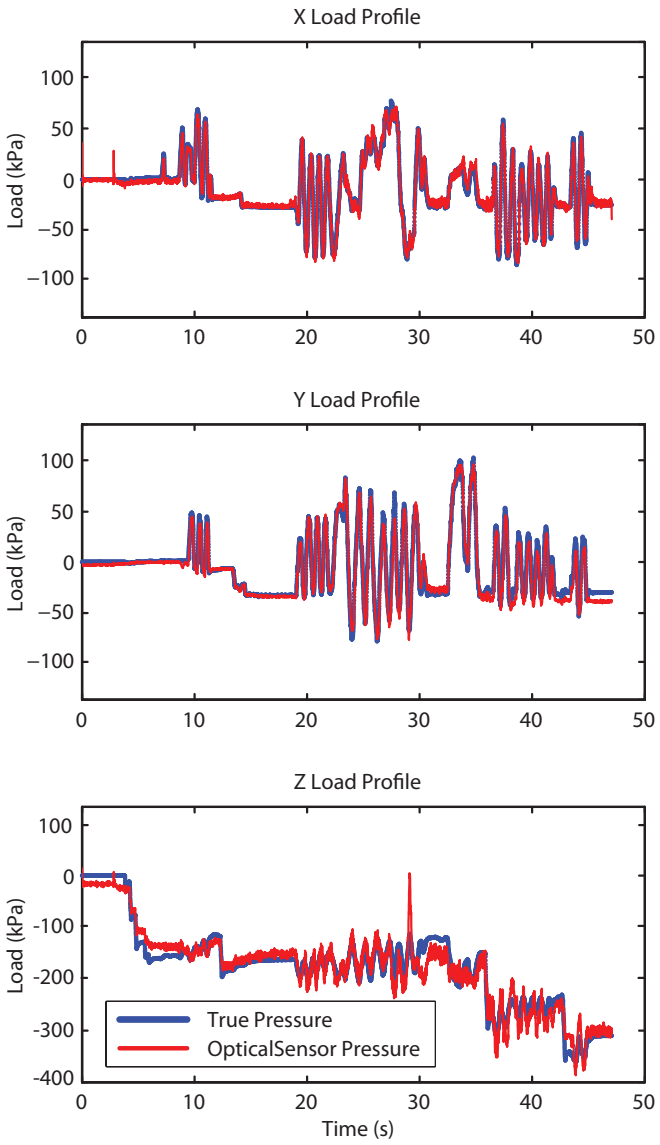

Fig. 9. Load profile showing truth and optical sensor load measurement in all three axis

response, the sensor had a significant response lag. The lag had no significant pure delay component, but consisted of viscoelastic-like behavior, almost certainly due to the silicone in its structure.

All three linear models provided reasonable pressure measurement performance. Surprisingly, the reduced-order models performed on par with the full 25 signal model. This has implications for the design of future generations of the sensor. Using three sensors instead of five will make taxels cheaper, smaller, and easier to fabricate. Using three signals instead of 25 will decrease the taxel's information demands, increasing its sampling rate and the amount of data the can be transmitted, processed, and stored or any given system.

The greatest opportunity for improving the taxel is in its sensitivity to normal loads. We plan to address this in two ways: 1) by making the sensor more sensitive to compression and 2) by refining the model of its operation. Preliminary data suggests that the sensitivity of the taxel to normal loads is highly dependent on the thickness of the transparent silicone (the clear resilient layer in Fig. 3). Thinner silicone appears to yield more sensitive taxels. The taxels evaluated in this paper all had a clear silicone thickness of 1-1.5mm. An initial analysis suggests that a 0.5mm-thick layer may yield normal sensitivities that are higher by a factor of 2-5.

We also plan to refine the model of the sensor beyond the linear models discussed above. Temperature compensation was not applied to these validation studies, but we have shown that it is an important component of error in environments where temperature is not controlled. And we have not yet examined models in which the three axes are dependent on one another. But likely the most important improvement we can make to our models is to explicitly account for hysteresis. The failure of the taxel to behave linearly is evident in the single-axis characterizations (see Fig. 7) and even in that simple case was responsible for a significant amount of error. By explicitly accounting for hysteresis in a model that retains a small amount of sensor history, we plan to reduce the error in all three sensing axes.

IV. ACKNOWLEDGMENTS

The authors would like to thank Jeff Dabling for assistance with the drift tests and Larry Anderson for assistance with the PCD design and fabrication. This work was funded in part by DARPA and the Congressionally-Directed Medical Research Program.

REFERENCES

[1] J. Ulmen and M. Cutkosky, "A robust, low-cost and low-noise artificial skin for human-friendly robots," *IEEE/RSJ International Conference on Intelligent Robots and Systems*, pp. 4836-4841, 2010.

[2] Y. Ohmura, A. Nagakubo, and Y. Kuniyshi, "Conformable and scalable tactile sensor skin for curved surfaces," *Proc. of the 2006 IEEE Int. Conf. on Robotics & Automation*, pp. 1348-1353, 2006.

[3] A. Dollar, C. R. Wagner, and R. D. Howe, "Embedded sensors for biomimetic robotics via shape deposition manufacturing," *Proceedings of the first IEEE/RAS-EMBS International Conference on Biomedical Robotics and Biomechatronics*, 2006.

[4] G. I. Rowe and A. V. Mamishev, "Simulation of a sensor array for multi-parameter measurements at the prosthetic limb interface," *PIE 9th Annual International Symposium on NDE for Health Monitoring and Diagnostics*, vol. 5394, pp. 493-500, 2004.

[5] M. R. Cutkosky, R. D. Howe, and W. R. Provancher, *Springer Handbook of Robotics*, ch. Force and Tactile Sensors, pp. 455-476. Berling/Heidelberg, Germany: Springer-Verlag, 2008.

[6] J. Sanders and C. Daly, "Measurement of stresses in 3 orthogonal directions at the residual limbprosthetic socket interface," *IEEE Trans Rehabil Eng*, vol. 1, pp. 79-85, 1993.

[7] K. Noda, K. Hoshino, K. Matsumoto, and I. Shimoyama, "A shear stress sensor for tactile sensing with the piezoresistive cantilever standing elastic material," *Sensors and Actuators A*, vol. 127, pp. 295-301, 2006.

[8] P. Valdastri, S. Roccella, E. C. L. Beccai, A. Menciassi, M. C. Carrozza, and P. Dario, "Characterization of a novel hybrid silicon three-axial force sensor," *Sens. Actuators A*, vol. 123124, pp. 249-257, 2005.

[9] Y.-M. Huang, N.-C. Tsai, and J.-Y. Lai, "Development of tactile sensors for simultaneous, detection of normal and shear stresses," *Sensors and Actuators*, vol. 159, pp. 189-195, 2010.

[10] J. Missinne, E. Bosman, B. V. Hoe, G. V. Steenberge, P. V. Daele, and J. Vanfleteren, "Embedded flexible optical shear sensor," *Proc. IEEE Sensors*, pp. 987-990, 2010.